

# Bridgeless PFC Boost Rectifier with Optimized Magnetic Utilization

Yungtaek Jang, Milan M. Jovanović, and David L. Dillman

Power Electronics Laboratory  
 Delta Products Corporation  
 P.O. Box 12173, 5101 Davis Drive  
 Research Triangle Park, NC 27709

**Abstract** — An implementation of bridgeless PFC boost rectifier with low common-mode noise is presented. The proposed implementation employs a unique multiple-winding, multi-core inductor to increase the utilization of the magnetic material. The operation and performance of the circuit was verified on a 750-W, universal-line experimental prototype operating at 110 kHz.

## I. INTRODUCTION

To maximize the power-supply efficiency, bridgeless PFC circuit topologies that may reduce the conduction loss by reducing the number of semiconductor components in the line-current path have been introduced [1] – [7]. Figures 1 through 4 show the bridgeless PFC boost implementations that have received the most attention. In each figure, the boost converter is implemented by replacing a pair of bridge rectifiers with switches and by employing an ac-side boost inductor. With a bridgeless topology, one rectifier is eliminated from the line-current path, which minimizes the conduction loss.

It should be noted that except the topology shown in Fig. 2, the other topologies can work both in CCM and DCM. The implementation in Fig. 2 that employs the totem-pole arrangement of the switches can only work in DCM because the reverse-recovery performance of the antiparallel diode makes CCM operation impractical.

The acceptance of the implementation in Fig. 1 in practical applications is hampered by a large common-mode noise produced by high-frequency switching of  $S_1$  and  $S_2$ , as explained and analyzed in [8] and [9]. The implementations in Figs. 2 through 4 does not suffer from the high common-mode noise problem, *i.e.*, they show common-mode noise characteristic identical to that of the conventional front-end architecture consisting of a full-bridge rectifier and conventional boost converter. As a result, these implementations are good candidates for applications in commercial products.

In this paper, a bridgeless PFC rectifier, also referred to as a dual boost converter, based on the implementation in Fig. 4 is described. The major drawback of the rectifier in Fig. 4 is the low utilization of switches and magnetic components. The proposed implementation employs a unique multiple-winding, multi-core inductor to increase the utilization of the

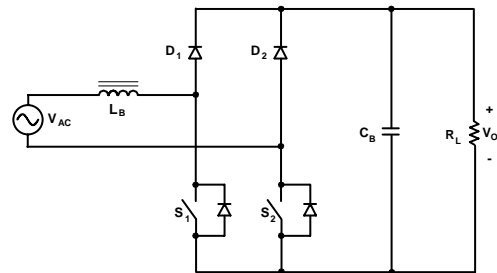


Fig. 1. Dual boost PFC rectifier [1].

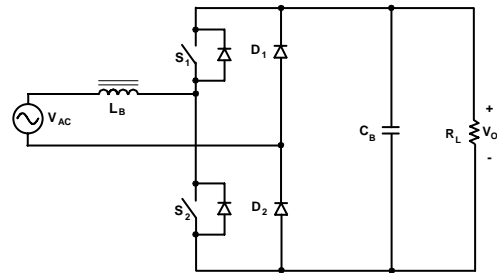


Fig. 2. Totem-pole dual boost PFC rectifier [5].

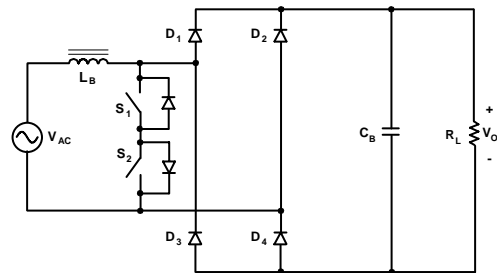


Fig. 3. Dual boost PFC rectifier with bi-directional switch [3].

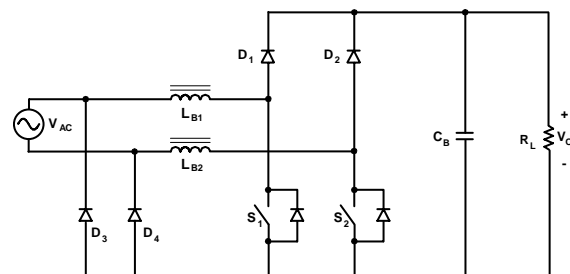


Fig. 4. Dual boost PFC rectifier with return diodes [6].

magnetic material. The operation and performance of the circuit was verified on a 750-W, universal-line experimental prototype operating at 110 kHz.

## II. DUAL BOOST PFC RECTIFIER WITH COMMON CORE INDUCTORS

The bridgeless PFC boost rectifier in Fig. 4 consists of two boost PFC rectifiers, each operating during a half line cycle. As indicated in Figs. 5 and 6, one boost rectifier operates while the other boost rectifier is idle. As a result, the utilization of switches and magnetic components is only one half of that of the conventional PFC boost converter that always utilizes all the components during the entire line cycle. The low utilization of the components may be a serious penalty in terms of weight, power density, and cost.

The utilization of the magnetics in the circuit in Fig. 4 can be significantly improved by employing a unique multiple-winding, multi-core inductor structure. The circuit diagram of this implementation of the dual boost PFC rectifier is shown in Fig. 7.

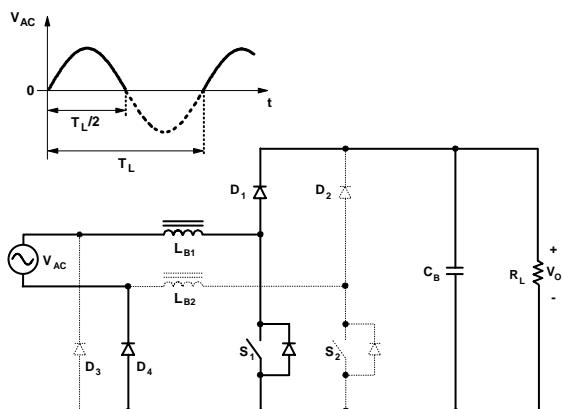


Fig. 5. Dual boost rectifier in Fig. 4 during the period when the line voltage is positive. The inactive components are shown in dashed lines.

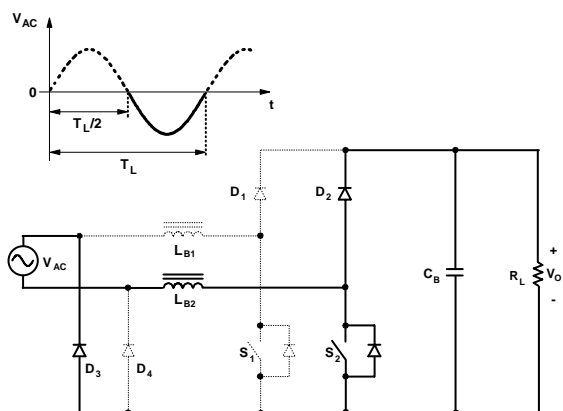


Fig. 6. Dual boost rectifier in Fig. 4 during the period when the line voltage is negative. The inactive components are shown in dashed lines.

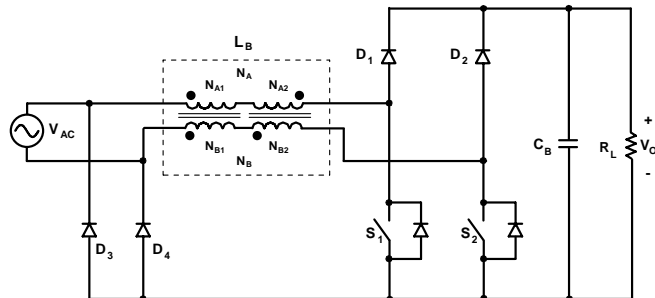


Fig. 7. Proposed dual boost PFC rectifier with common-core inductors.

### A. Multi-Port Magnetic Elements with Decoupled Energy Storage

As shown in Fig. 8, boost inductor  $L_B$  consists of a first winding, a second winding, and two cores. The first winding ( $N_A$ ) consists of series connected windings  $N_{A1}$  and  $N_{A2}$ . The second winding ( $N_B$ ) consists of series connected windings  $N_{B1}$  and  $N_{B2}$ . Windings  $N_{A1}$  and  $N_{B1}$  are wound on the first core in the same direction. However, windings  $N_{A2}$  and  $N_{B2}$  are wound on the second core in opposite directions.

To facilitate the explanation of the magnetic element, Fig. 9 shows the simplified symbol of the integrated magnetic device in Fig. 8 with the polarity mark of each winding. Moreover, Fig. 10 shows the integrated magnetic device in Fig. 8 with reference directions of currents and magnetic flux as current  $i_A$  flows through winding  $N_A$ . To make the two windings magnetically independent of each other, windings  $N_{A1}$  and  $N_{A2}$  should have an equal number of turns, *i.e.*,  $N_{A1}=N_{A2}$ . In addition, windings  $N_{B1}$  and  $N_{B2}$  should also have an equal number of turns, *i.e.*,  $N_{B1}=N_{B2}$ . As can be seen in Fig. 10, current  $i_A$  generates magnetic flux  $\phi_A=N_A \times i_A$  in each core. The change of flux  $\phi_A$  induces the current in windings  $N_{B1}$  and  $N_{B2}$  in each core. Because of the opposite winding

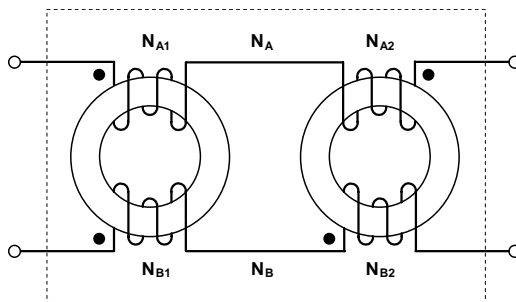


Fig. 8. Two-winding integrated magnetic device with the decoupled energy storage.

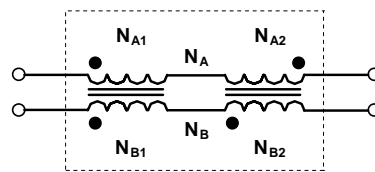


Fig. 9. Simplified symbol of the magnetic device shown in Fig. 8.

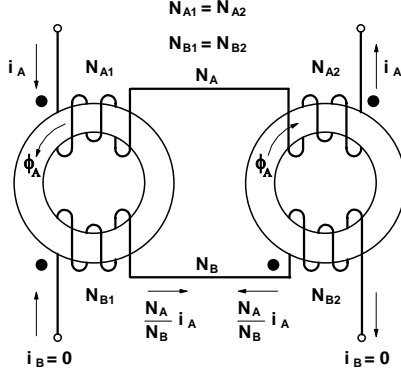


Fig. 10. Integrated magnetic device in Fig. 8 with reference directions of currents and magnetic flux as current  $i_A$  flows through winding  $N_A$ .

directions and the equal number of turns of  $N_{B1}$  and  $N_{B2}$ , the induced currents in windings  $N_{B1}$  and  $N_{B2}$  have opposite directions and equal magnitudes. As a result, the total current of winding  $N_B$  is zero, *i.e.*,  $i_B=0$ . Similarly, current  $i_A$  is zero when current  $i_B$  flows in winding  $N_B$ . As a result, the first winding and the second winding are magnetically independent and can be used as two different inductors.

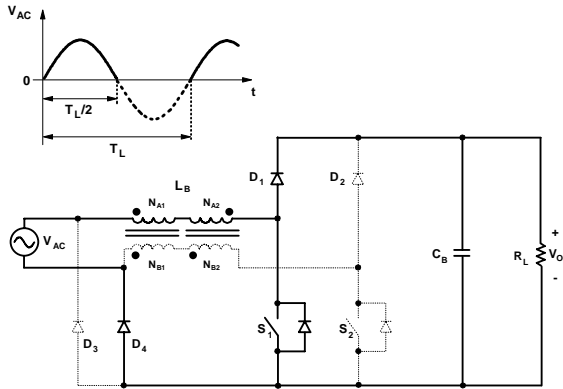


Fig. 11. Dual boost rectifier with common core inductors in Fig. 7 during the period when the line voltage is positive. The inactive components are shown in dashed lines.

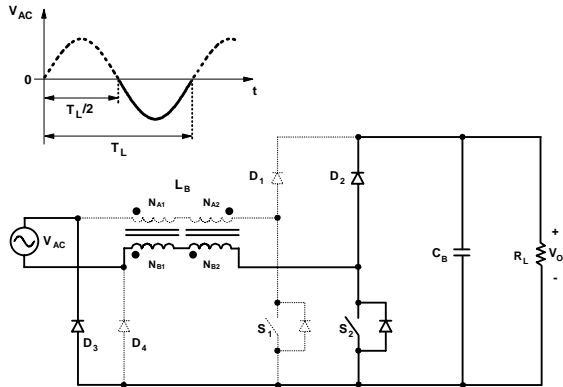


Fig. 12. Dual boost rectifier with common core inductors in Fig. 7 during the period when the line voltage is negative. The inactive components are shown in dashed lines.

### B. Dual Boost PFC Rectifier with Common-Core Inductors

Figure 7 shows the dual-boost PFC rectifier with the two-winding integrated magnetic device shown in Fig. 8. By using the proposed technique, the two separate boost inductors of the dual boost PFC front-end rectifier can be integrated. As shown in Fig. 11, during the period when ac input voltage  $V_{AC}$  is positive, the boost rectifier that consists of switch  $S_1$ , diodes  $D_1$  and  $D_4$ , and windings  $N_{A1}$  and  $N_{A2}$  operates to deliver energy to the output, while the boost rectifier that consists of switch  $S_2$ , diodes  $D_2$  and  $D_3$ , and windings  $N_{B1}$  and  $N_{B2}$  is idle. It should be noted that the two cores on which windings  $N_{A1}$  and  $N_{A2}$  are wound are fully utilized although windings  $N_{B1}$  and  $N_{B2}$  are idle. Similarly, during the period when ac input voltage  $V_{AC}$  is negative as shown in Fig. 12, the boost rectifier that consists of switch  $S_2$ , diodes  $D_2$  and  $D_3$ , and windings  $N_{B1}$  and  $N_{B2}$  operates to deliver energy to the output, while the boost rectifier that consists of switch  $S_1$ , diodes  $D_1$  and  $D_4$ , and windings  $N_{A1}$  and  $N_{A2}$  is idle. It should be also noted that the two cores are still fully utilized by windings  $N_{B1}$  and  $N_{B2}$  although windings  $N_{A1}$  and  $N_{A2}$  are idle. As a result, the high utilization of the magnetic cores significantly improves power density and reduces the overall weight of the power supply.

Figure 13 shows another application of the proposed technique. The two-winding integrated magnetic device shown in Fig. 8 is employed in a dual cascaded buck and boost rectifier. During the period when ac input voltage  $V_{AC}$  is positive and greater than output voltage  $V_O$ , the buck converter that consists of switch  $S_1$ , diodes  $D_1$  and  $D_6$ , and windings  $N_{A1}$  and  $N_{A2}$  operates to deliver energy to the output through diode  $D_3$ . It should be noted that the two cores are fully utilized by windings  $N_{A1}$  and  $N_{A2}$  to form a buck filter inductor. During the period when ac input voltage  $V_{AC}$  is positive and smaller than output voltage  $V_O$ , the boost converter that consists of switch  $S_3$ , diodes  $D_3$  and  $D_6$ , and windings  $N_{A1}$  and  $N_{A2}$  operates to deliver energy to the output through switch  $S_1$  that is continuously turned on during this period. It should also be noted that the two cores are fully utilized by windings  $N_{A1}$  and  $N_{A2}$  to form a boost inductor. During the period when ac input voltage  $V_{AC}$  is negative and its magnitude is greater than output voltage  $V_O$ , the buck converter that consists of switch  $S_2$ , diodes  $D_2$  and  $D_5$ , and

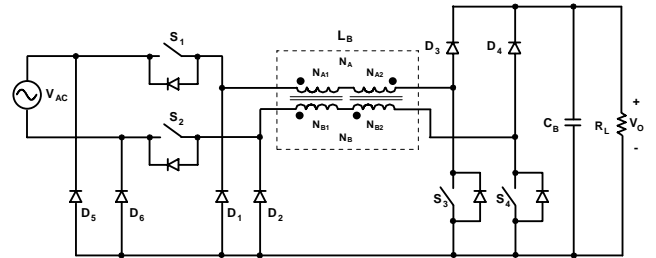


Fig. 13. Proposed dual cascaded buck and boost PFC rectifier with common-core inductors.

windings  $N_{B1}$  and  $N_{B2}$  operates to deliver energy to the output through diode  $D_4$ . It should be noted that the two cores are fully utilized by windings  $N_{B1}$  and  $N_{B2}$  to form a buck filter inductor. During the period when ac input voltage  $V_{AC}$  is negative and its magnitude is smaller than output voltage  $V_O$ , the boost converter that consists of switch  $S_4$ , diodes  $D_4$  and  $D_5$ , and windings  $N_{B1}$  and  $N_{B2}$  operates to deliver energy to the output through switch  $S_2$  that is continuously turned on during this period. It should be also noted that the two cores are fully utilized by windings  $N_{B1}$  and  $N_{B2}$  to form a boost inductor.

### III. EXPERIMENTAL RESULTS

The performance of the proposed rectifier shown in Fig. 7 was evaluated on a 110-kHz, 750-W prototype circuit that was designed to operate from a universal ac-line input (85  $V_{RMS}$ -264  $V_{RMS}$ ) and deliver up to 1.97 A at a 400-V output. Since the drain voltage of boost switches  $S_1$  and  $S_2$  is clamped to bulk capacitor  $C_B$ , the peak voltage stress on each boost switch is approximately 400 V. The peak current stress on boost switches  $S_1$  and  $S_2$ , which occurs at full load and low line, is approximately 13.3 A. Therefore, an IPP60R099CS MOSFET ( $V_{DSS} = 600$  V,  $I_{D25} = 19$  A,  $R_{DS} = 0.099 \Omega$ ) from Infineon was used as each boost switch. Boost diodes  $D_1$  and  $D_2$  were implemented with SDT08S60 SiC diode ( $V_{RRM} = 600$  V,  $I_{FAVM} = 8$  A) from Infineon and two diodes of a bridge rectifier D15XB60 ( $V_{RRM} = 600$  V,  $I_{FAVM} = 15$  A) from Shindengen were used as diodes  $D_3$  and  $D_4$ .

The structure of the common-core inductors is shown in Fig. 8. The cores of inductor  $L_B$  are 58928-A2 (high flux core,  $\mu=160$ ,  $OD=1.09''$ ) from Magnetics. A magnet wire (30 turns, AWG# 16) was used for each winding of  $N_{A1}$ ,  $N_{A2}$ ,  $N_{B1}$ , and  $N_{B2}$ . Two high-voltage aluminum capacitors (470  $\mu F$ , 450 VDC) were used for bulk capacitor  $C_B$ .

An ICE1PCS01 (8-pin continuous-conduction-mode PFC controller) from Infineon was used in the experimental prototype circuit because it does not require line voltage information. If a conventional PFC controller were used, such as UCC3854, a relatively complex input voltage sensing circuit would be required. It should be noted that switches  $S_1$  and  $S_2$  are operated simultaneously by the same gate signal from the controller. Although both switches are always gated, only one switch, on which the positive input voltage is induced, *i.e.*, switch  $S_1$  in Fig. 11, carries positive current and delivers the power to the output. The other switch, on which the negative input voltage is induced, *i.e.*, switch  $S_2$  in Fig. 11, doesn't influence the operation since its body diode that is effectively connected in parallel with  $D_4$  conducts.

To compare the performance of the proposed rectifier and conventional PFC rectifiers, same prototype hardware was used. To measure the efficiency of the conventional dual boost PFC rectifier with return diodes shown in Fig. 4, common core inductor  $L_B$  of the proposed rectifier was replaced by two inductors. Each inductor consisted of two 58928-A2 high-flux cores and a magnet wire (52 turns, AWG# 16). Moreover, to measure the efficiency of the

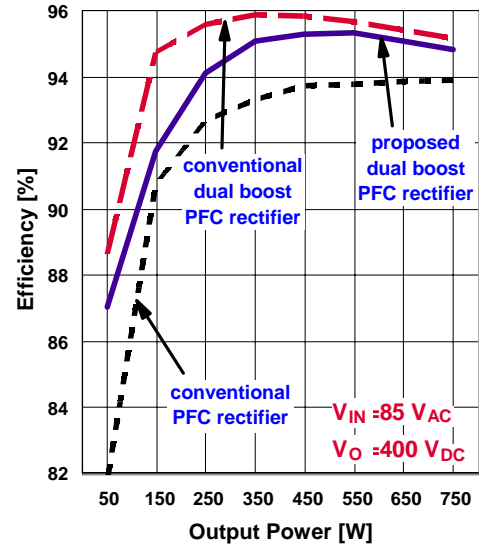


Fig. 14. Measured efficiencies of conventional PFC rectifier (dotted line), dual boost PFC rectifier with return diodes in Fig. 4 (dashed line), and proposed dual boost PFC rectifier with common core inductors in Fig. 7 (solid line) as functions of output power.

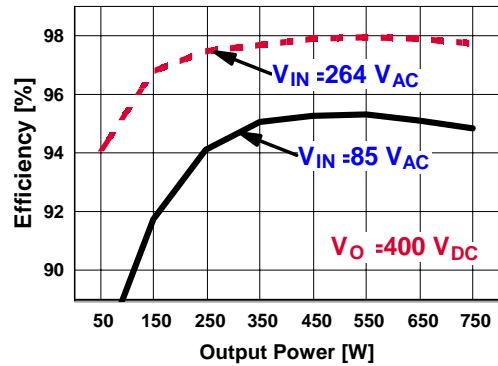


Fig. 15. Measured efficiency of proposed dual boost PFC rectifier with common core inductors at  $V_{IN}=85$   $V_{AC}$  (solid line) and  $V_{IN}=264$   $V_{AC}$  (dashed line) as functions of output power.

conventional boost PFC circuit with input bridge rectifier, two IPP60R099CS MOSFETs connected in parallel were used as its boost switch, while two SDT08S60 SiC diodes connected in parallel were used as its boost diode. A full-bridge rectifier D15XB60 ( $V_{RRM} = 600$  V,  $I_{FAVM} = 15$  A) from Shindengen was used as an input bridge rectifier. The boost inductor consisted of two 58928-A2 high-flux cores and a magnet wire (52 turns, AWG# 16).

Figure 14 shows the measured efficiency of the proposed dual boost PFC rectifier with common-core inductors (solid line), the conventional dual boost PFC rectifier (dashed line), and the conventional PFC boost rectifier (dotted line) as functions of the output power. As can be seen in Fig. 14, the bridgeless rectifiers have higher conversion efficiency than the conventional boost PFC rectifier over the entire measured power range. It should be noted that the proposed bridgeless PFC rectifier with common core inductors has slightly lower

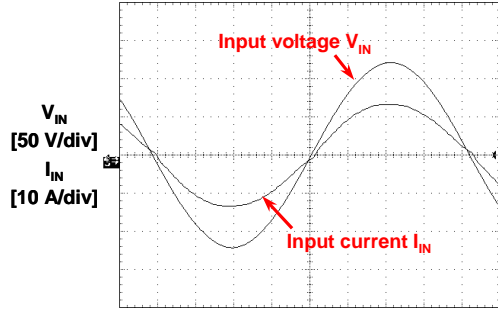


Fig. 16. Measured input voltage and current waveforms of the proposed circuit at  $V_{IN}=85$  V<sub>AC</sub>,  $V_O=400$  V<sub>DC</sub>,  $P_O=750$  W. PF=99.9%, THD=3.5%. Time base: 2 ms/div.

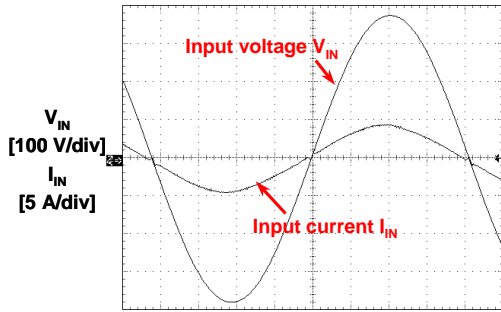


Fig. 17. Measured input voltage and current waveforms of the proposed circuit at  $V_{IN}=264$  V<sub>AC</sub>,  $V_O=400$  V<sub>DC</sub>,  $P_O=750$  W. PF=99.1%, THD=7.9%. Time base: 2 ms/div.

efficiency than the conventional dual boost PFC rectifier in Fig. 4. The proposed technique improves the efficiency by approximately 1% at 750 W, which translates into approximately 17% reduction of losses. Figure 15 shows the measured efficiency of the proposed dual boost PFC rectifier with common-core inductors at  $V_{IN}=85$  V<sub>AC</sub> (solid line) and  $V_{IN}=264$  V<sub>AC</sub> (dashed line).

Figures 16 and 17 show the measured input voltage and the current waveforms at  $V_{IN}=85$  V<sub>AC</sub>, and  $V_{IN}=264$  V<sub>AC</sub>, respectively. The measured total harmonic distortion (THD) and power factor (PF) of the converter at low line and high line are plotted in Figs. 18 and 19, respectively. The measured THD and PF of the proposed rectifier at minimum line and full load are approximately 3.5% and 99.9%, respectively while those at maximum line and full load are approximately 7.9% and 99.1%, respectively.

#### IV. SUMMARY

The dual boost PFC rectifier that employs a multiple-winding magnetic device to increase the utilization of the magnetic core has been introduced. The performance of the proposed rectifier was verified on a 750-W experimental prototype. The measured efficiency and THD of the converter at minimum line and full load are approximately 94.9% and 3.5%, respectively. The proposed technique improves the efficiency by approximately 1% compared to the conventional PFC boost rectifier, and improves the utilization of the magnetic cores from the conventional bridgeless dual boost rectifier, resulting in a lower-cost high-power-density design.

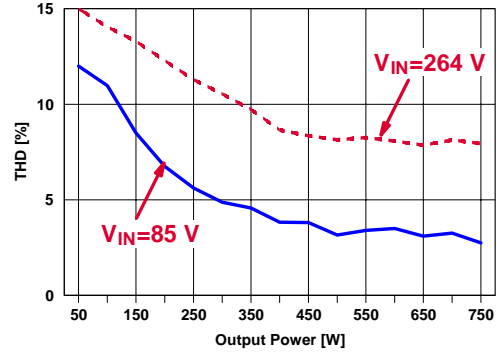


Fig. 18. Measured THD of proposed dual boost PFC rectifier with common core inductors at  $V_{IN}=85$  V<sub>AC</sub> (solid line) and  $V_{IN}=264$  V<sub>AC</sub> (dashed line) as function of output power.

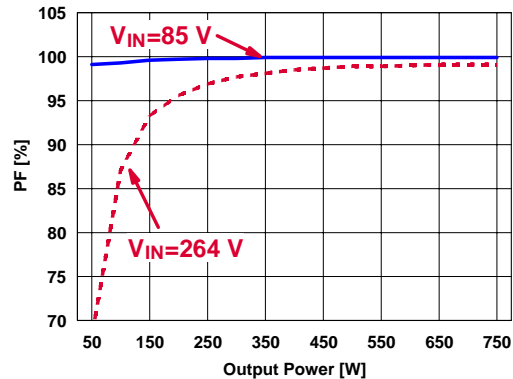


Fig. 19. Measured PF of proposed dual boost PFC rectifier with common core inductors at  $V_{IN}=85$  V<sub>AC</sub> (solid line) and  $V_{IN}=264$  V<sub>AC</sub> (dashed line) as function of output power.

#### REFERENCES

- [1] D.M. Mitchell, "AC-DC Converter having an improved power factor", U.S. Patent 4,412,277, Oct. 25, 1983.
- [2] J.C. Salmon, "Circuit topologies for single-phase voltage-doubler boost rectifiers," *IEEE Applied Power Electronics (APEC) Conf. Proc.*, pp. 549-556, Mar. 1992.
- [3] D. Tollik, A. Pietkiewicz "Comparative analysis of 1-phase active power factor correction topologies," *International Telecommunication Energy Conf. (INTELEC) Proc.*, pp. 517-523, Oct. 1992.
- [4] A.F. Souza and I. Barbi, "A new ZVS-PWM unity power factor rectifier with reduced conduction losses," *IEEE Trans. Power Electronics*, vol. 10, No. 6, pp. 746-752, Nov. 1995.
- [5] J.C. Salmon, "Circuit topologies for PWM boost rectifiers operated from 1-phase and 3-phase ac supplies and using either single or split dc rail voltage outputs," *IEEE Applied Power Electronics (APEC) Conf. Proc.*, pp. 473-479, Mar. 1995.
- [6] A.F. Souza and I. Barbi, "High power factor rectifier with reduced conduction and commutation losses," *International Telecommunication Energy Conf. (INTELEC) Proc.*, Session 8, paper 1, Jun. 1999
- [7] T. Ernő and M. Frisch, "Second generation of PFC solutions," *Power Electronics Europe*, Issue 7, pp. 33-35, 2004.
- [8] H. Ye, Z. Yang, J. Dai, C. Yan, X. Xin, and J. Ying, "Common mode noise modeling and analysis of dual boost PFC circuit," *International Telecommunication Energy Conf. (INTELEC) Proc.*, pp. 575-582, Sep. 2004.
- [9] B. Lu, R. Brown, and M. Soldano, "Bridgeless PFC implementation using one cycle control technique," *IEEE Applied Power Electronics (APEC) Conf. Proc.*, pp. 812-817, Mar. 2005.